



Original scientific paper

Experimental and theoretical study on corrosion inhibition of mild steel by meso-tetraphenyl-porphyrin derivatives in acid solution

Messaoud Meraghni^{1,2}, Touhami Lanez^{2,✉}, Elhafnaoui Lanez², Lazhar Bechki³ and Ali Kennoufa²

¹University of El Oued, Process Engineering Department, Faculty of Technology, B.P.789, 39000, El Oued, Algeria

²VTRS Laboratory, Department of Chemistry, Faculty of Sciences, University of El Oued B.P.789, 39000, El Oued, Algeria

³University of Ouargla, Chemistry Department, PO Box 511, 30000, Ouargla, Algeria

Corresponding author: ✉ touhami-lanez@univ-elourd.dz

Received: June 12, 2022; Accepted: August 23, 2022; Published: August xx, 2022

Abstract

The inhibition effect of meso-tetraphenyl-porphyrin (TPPH₂), meso-tetra4-methophenyl-porphyrin TPPH₂(p-Me), and meso-tetra4-actophenyl-porphyrin (TAcPPH₂) on the corrosion of XC52 mild steel in aerated 0.5 M aqueous sulfuric acid solution was studied by potentiodynamic polarization experiments and quantum chemical calculations. Results from potentiodynamic polarization showed that inhibition efficiency of three compounds increased upon increasing of the inhibitor concentration and they are acting as mixed type inhibitors, having dominant anodic reactions. Adsorption of all compounds follows the Langmuir adsorption isotherm with moderate values of free energy of adsorption. Quantum chemical calculation using DFT/B3LYP method confirmed a strong bond between meso-tetraphenyl-porphyrins and mild steel surface. The inhibition mechanism was also determined by the potential of zero charge (PZC) measurement at the metal/solution interface.

Keywords

Low carbon steel; potentiodynamic polarization; quantum chemical method, potential of zero charge

Introduction

Mild steel is made from iron with low carbon content of approximately 0.05-0.30 % by weight, where other elements such as manganese and silicon may be also added. The presence of carbon content improves toughness and corrosion-resistance of mild steel compared to pure iron. Mild steel is one of the most widely used materials in industry such as electronics, and the manufacture

of integrated circuits, as well as a construction material for pipeline transport production and processing related industries [1,2].

As many other metals, mild steel is usually exposed to corrosion in various industries. These exposures can make changes in the properties of the metals and thus to unexpected failures of materials in service. Therefore, a metal surface should be protected from corrosion attack, and the most efficient method of metal protection against aqueous acidic corrosion is utilization of organic inhibitors molecules.

Despite the fact that mild steel has numerous applications, it shows weak resistance to corrosion attack in corrosive aqueous media [3-5]. Consequently, the development of protective materials able to increase the corrosion resistance of mild steel is mandatory. In this case also, the use of organic compounds as corrosion inhibitors is one of the most widespread protective methods against aqueous corrosion.

Organic inhibitors are usually organic molecules containing heteroatoms such as nitrogen, oxygen and sulphur that result in the enhanced adsorption onto a metal surface [6,7]. Also, the presence of aromatic cycles and aliphatic chains in the molecular structures of inhibitors improve their adsorption at a metal surface. In such a manner, a metal surface becomes isolated from the corrosive media and consequently, its corrosion resistance is improved [8,9].

Porphyrins are a class of cyclic tetrapyrroles which possess a highly conjugated, heterocyclic macrocycle. Their 18π electron structure gives rise to their remarkable stability, their structures are formed by four pyrrole subunits connected together *via* methine bridges. The presence of four nitrogen atoms in their skeletons qualifies them to be potential corrosion inhibitors. Additionally, the fully aromatic character of meso-tetraphenyl-porphyrin derivatives facilitates the mobility of electrons in the rings, which makes possible their application in many fields such as electrochemistry and catalysis [9], photomedicine [10] and photosynthesis [11].

In the present work, the corrosion inhibition efficiency of 5,10,15,20-tetraphenylporphyrin (TPPH₂), 5,10,15,20-tetra-p-tolylporphyrin (TPPH₂(p-Me)), and 1,1',1'',1'''-(porphyrin-5,10,15,20-tetra-yltetrakis(benzene-4,1-diyl))tetrakis(ethan-1-one) (TAcPPH₂) on XC52 steel in sulfuric acid solution has been studied using potentiodynamic polarization measurements and quantum chemical calculations.

Experimental

Materials and sample preparation

Sulfuric acid (Sigma Aldrich) used as corrosive medium in this study was of analytical grade and used as sourced without further preparation.

The chemical composition of the XC52 mild steel used in this study is: 0.065 wt.% C, 0.245 wt.% Si, 1.685 wt.% Mn, 0.002 wt.% P, 0.001 wt.% S, 0.042 wt.% Cr, 0.005 wt.% Cr, 0.026 wt.% Ni, 0.042 wt.% Al, 0.010 wt.% Cu, 0.067 wt.% Nb, 0.019 wt.% Ti, 0.014 wt.% V and the remainder Fe. It was obtained as platelets from ANABIB Ltd (Ghardaïa, Algeria).

Electrochemical measurements

The electrochemical measurements were conducted on a PGZ301 potentiostat (radiometer analytical SAS, France) connected to a standard three-electrode electrochemical cell assembly composed of a saturated calomel electrode (Hg/Hg₂Cl₂/Cl⁻) and a platinum wire as the reference and auxiliary electrode, respectively. Mild steel (XC52) rod with 0.707 cm² of exposed surface area served as the working electrode. All experiments were performed in atmospheric conditions

without stirring. Prior to each assay, the working electrode was immersed in the test solution until a stable value for the open circuit potential was obtained (40 to 60 minutes).

Synthesis

The synthesis of meso-tetraphenyl-porphyrin derivatives (TPPH₂, TPPH₂(p-Me), and TAcPPH₂) used in this work as potential inhibitors of corrosion of XC52 mild steel in aqueous sulfuric acid solution, was performed following our previously reported procedure [10]. Molecular structures of three synthesized porphyrin derivatives are shown in Figure 1.

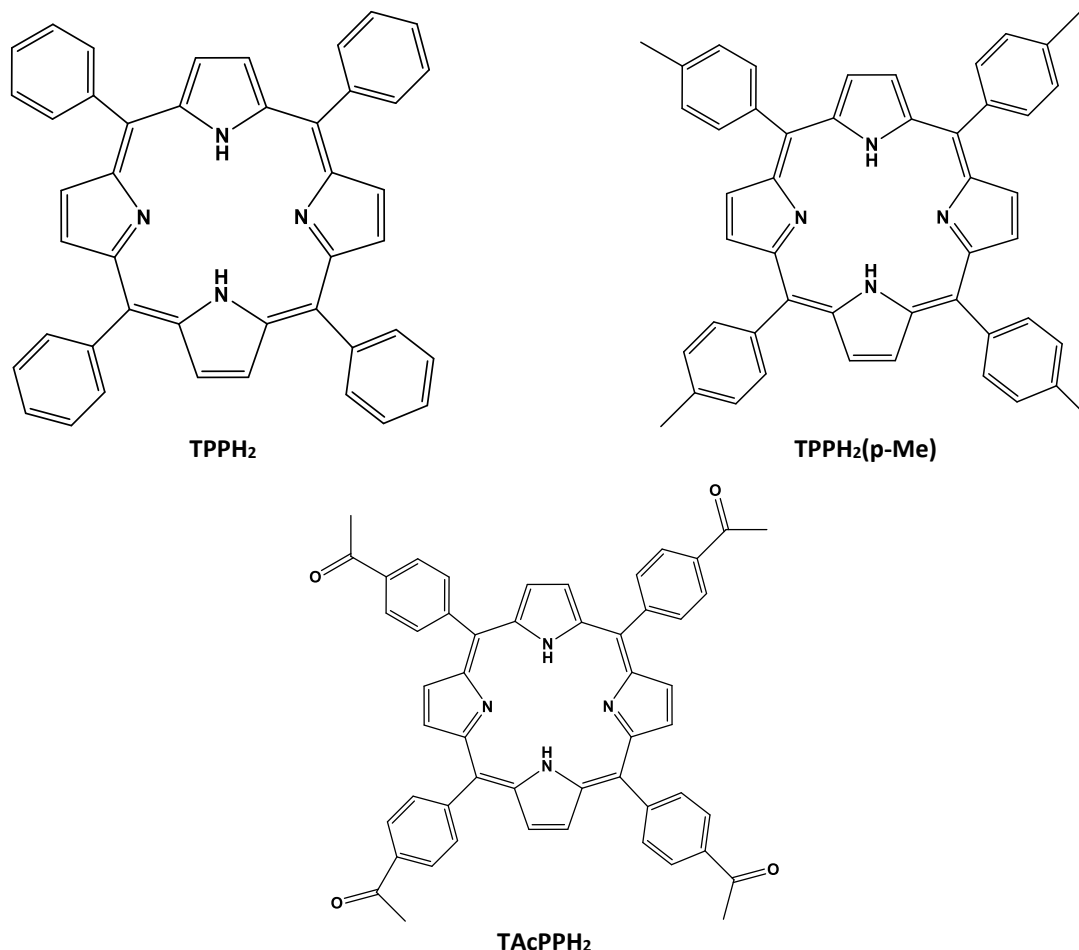


Figure 1. Chemical structures of meso-tetraphenyl-porphyrin derivatives

A stock solution of each inhibitor (300 ppm) was prepared by weighing 300 mg of synthesized material dissolved in one liter of 0.5M sulfuric acid. Other concentrations (10 – 100 ppm) were obtained from the stock solution following successive dilution.

The XC52 mild steel electrode used for electrochemical assays was prepared, degreased, and cleaned as previously reported [11,12].

Structure optimizations were run using density functional theory (DFT) implemented in Gaussian 09 package [13]. All calculations were carried out with the unrestricted Becke's three parameter hybrid exchange functional [14] combined with Lee-Yang-Parr nonlocal correlation function, abbreviated as B3LYP [15–17] with basis set 6-311++G(d,p) [18–20].

Results and discussion

Potentiodynamic polarization study

Potentiodynamic polarization curves were used to study the corrosion inhibition of XC52 mild steel in aerated 0.5 M aqueous sulfuric acid solution, in the absence and presence of different concentrations of TPPH₂, TPPH₂(p-Me), and TAcPPH₂ at 25±1 °C. The obtained Tafel curves are shown in Figure 2.

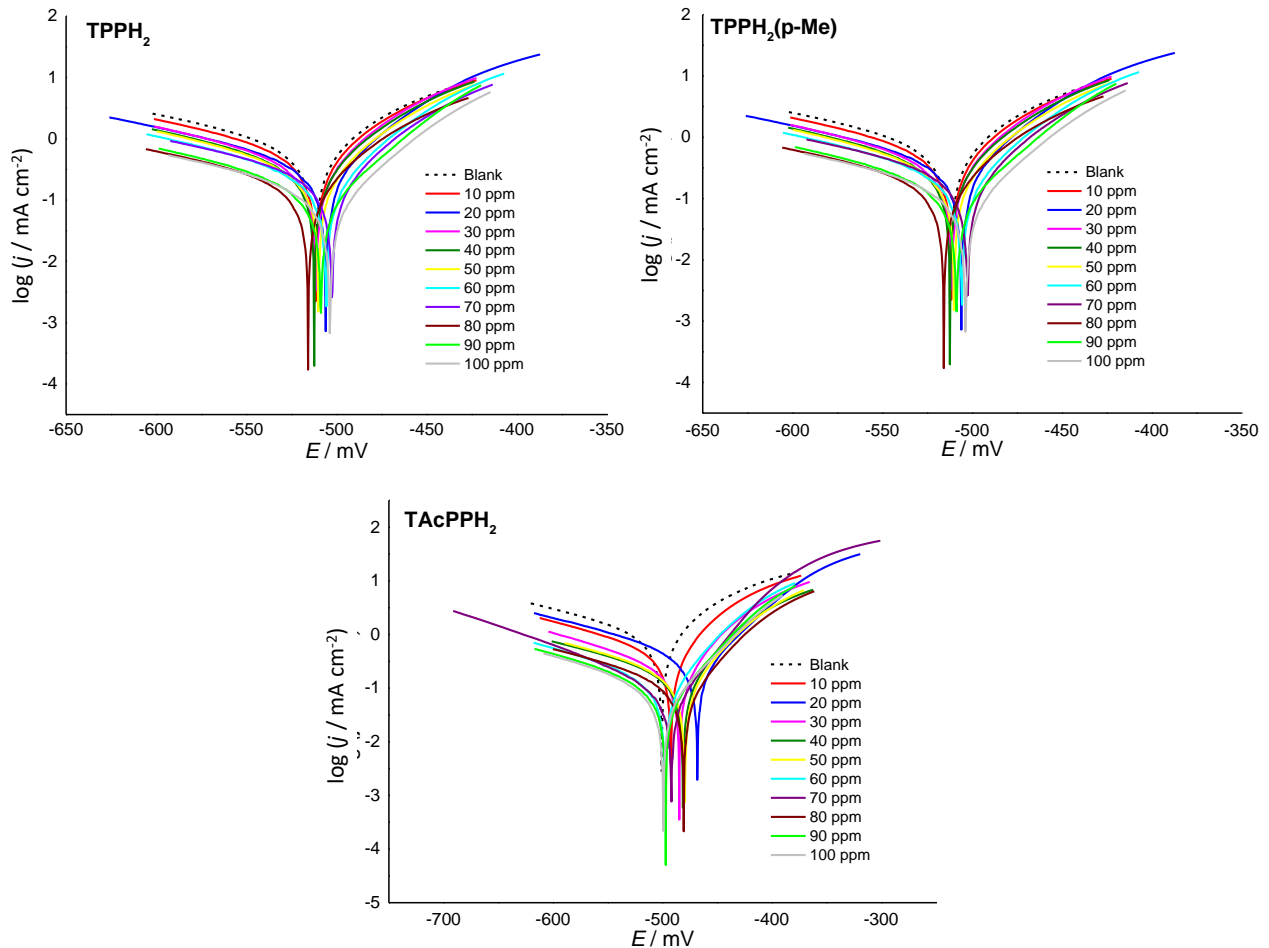


Figure 2. Potentiodynamic polarization curves of mild steel in 0.5 M H₂SO₄ in the absence (blank) and presence of different (10-100 ppm) concentrations of TPPH₂, TPPH₂(p-Me) and TAcPPH₂

Figure 2 shows that in the presence of inhibitors, all anodic Tafel slopes were lower compared to the blank solution, thus showing the effect of the inhibitors on the metal dissolution reaction. In contrast, cathodic Tafel slopes were less affected. This infers that compounds in the present study were inhibitors of mixed type, having dominant anodic reaction [21].

The corrosion current densities were determined from the intersection of anodic and cathodic Tafel slopes, while inhibition efficiency (*IE* / %) was calculated from the corrosion current density of XC52 mild still electrodes in the absence and presence of the inhibitor using the equation (1) [22]:

$$IE = \left(\frac{j_0 - j}{j_0} \right) 100 \tag{1}$$

where *j*₀ and *j* are the current density values in the absence and presence of inhibitor respectively. Corrosion current density values and *IE* calculated by eq. (1), are for different concentrations (10-100 ppm) of three inhibitors presented in Table 1.

Table 1. Inhibition efficiencies of different concentrations of TPPH₂, TPPH₂(p-Me), and TAcPPH₂ inhibitors toward XC52 mild steel corrosion in 0.5 M H₂SO₄

C / ppm	TPPH ₂		TPPH ₂ (p-Me)		TAcPPH ₂	
	j / mA cm ⁻²	IE / %	j / mA cm ⁻²	IE / %	j / mA cm ⁻²	IE / %
--	0.6727	--	0.6727	--	0.6727	--
10	0.4311	36	0.4039	40	0.4002	41
20	0.3988	41	0.3908	42	0.3142	53
30	0.3669	45	0.3621	46	0.2075	69
40	0.3308	51	0.3284	51	0.1808	73
50	0.3003	55	0.2915	57	0.178	74
60	0.2502	63	0.2414	64	0.1341	80
70	0.2365	65	0.2313	66	0.1279	81
80	0.2283	66	0.2194	67	0.1223	82
90	0.2194	67	0.2091	69	0.1097	84
100	0.2088	69	0.1988	70	0.1031	85

It is clearly seen from Table 1 that the current density values decrease considerably with increasing concentration of the inhibitors due to the formation of a barrier film on the mild steel surface. Moreover, for all three inhibitors, inhibition efficiency increases with concentration, while the maximum IE of 85 % is observed for 100 ppm of TAcPPH₂, indicating significant protection of the mild steel from corrosion.

Anodic and cathodic Tafel slopes

As shown in Table 2, in solutions without and with different concentrations of inhibitors, the values of anodic Tafel slope (β_a) varied from 48 to 72 mV for TPPH₂, from 52 to 71 mV for TPPH₂(p-Me), and from 48 to 80 mV for TAcPPH₂. The values of cathodic slopes (β_c) varied from -121 to -160 mV for TPPH₂, from -135 to -193 mV for TPPH₂(p-Me), and from -149 to -194 mV for TAcPPH₂. These limits represent typical anodic and cathodic Tafel slopes that were reported in the literature for mild steel in acidic solutions [23,24]. As it can be observed from Table 1 and 2, the variations of anodic and cathodic Tafel slopes caused by the addition of the inhibitors, affected both the corrosion potential and the anodic and cathodic current densities.

As β_a increases, the potential on the anodic mild steel surface also increases; however, the potential distribution along the cathodic surface is not affected significantly. Therefore, as β_a increases, the potential difference between the anodic and cathodic regions decreases, and this results in lower corrosion rates.

Table 2. Anodic and cathodic Tafel slopes for the mild steel immersed in 0.5 M H₂SO₄ medium for 30 min

C / ppm	TPPH ₂			TPPH ₂ (p-Me)			TAcPPH ₂		
	E _{corr} / mV	β_a / mV dec ⁻¹	β_c / mV dec ⁻¹	E _{corr} / mV	β_a / mV dec ⁻¹	β_c / mV dec ⁻¹	E _{corr} / mV	β_a / mV dec ⁻¹	β_c / mV dec ⁻¹
00	-516	72	-154	-503	71	-183	-501	80	-188
10	-511	65	-150	-499	66	-193	-492	63	-183
20	-506	56	-140	-497	61	-173	-468	69	-191
30	-511	56	-140	-493	63	-187	-485	56	-160
40	-512	57	-140	-495	61	-192	-481	61	-194
50	-510	56	-138	-493	59	-185	-480	62	-185
60	-505	53	-137	-489	58	-176	-498	57	-165
70	-503	54	-141	-507	64	-156	-492	53	-149
80	-512	56	-135	-490	57	-182	-480	60	-185
90	-509	53	-137	-487	52	-154	-497	60	-170
100	-504	48	-121	-498	55	-135	-499	48	-175

Adsorption isotherm

In order to find out the mode of adsorption of three porphyrin derivative inhibitors on the surface of XC52 mild steel and the adsorption isotherm that fits the experimental results, the θ/C_{inh} values were plotted versus inhibitor concentration (C_{inh}) for all investigated compounds (Figure 3). The obtained straight lines follow the Langmuir adsorption isotherm that is given by the equation (2) [25]:

$$\frac{C_{inh}}{\theta} = C_{inh} + \frac{1}{K_{ads}} \tag{2}$$

where θ is surface coverage degree, C_{inh} is concentration of tested inhibitor compounds, and K_{ads} is adsorption equilibrium constant.

The surface coverage degree (θ) was calculated based on the assumption that the inhibition efficiency (IE) is due mainly to the blocking effect of the adsorbed inhibitor molecules on the metal surface. Hence, θ is given by the equation (3) [26]:

$$\theta = \frac{IE}{100} = 1 - \frac{j}{j_0} \tag{3}$$

The values of adsorption equilibrium constant (K_{ads}) obtained from intercepts of linear lines at θ/C_{inh} axes in Figure 3, are listed in Table 3. The results demonstrate that all values of the linear correlation coefficients (R^2) and all slopes are almost equal to one, which confirms that adsorption of all three studied inhibitor molecules in 0.5 M aqueous sulfuric acid on the surface of the X52 mild steel obeys Langmuir adsorption isotherm.

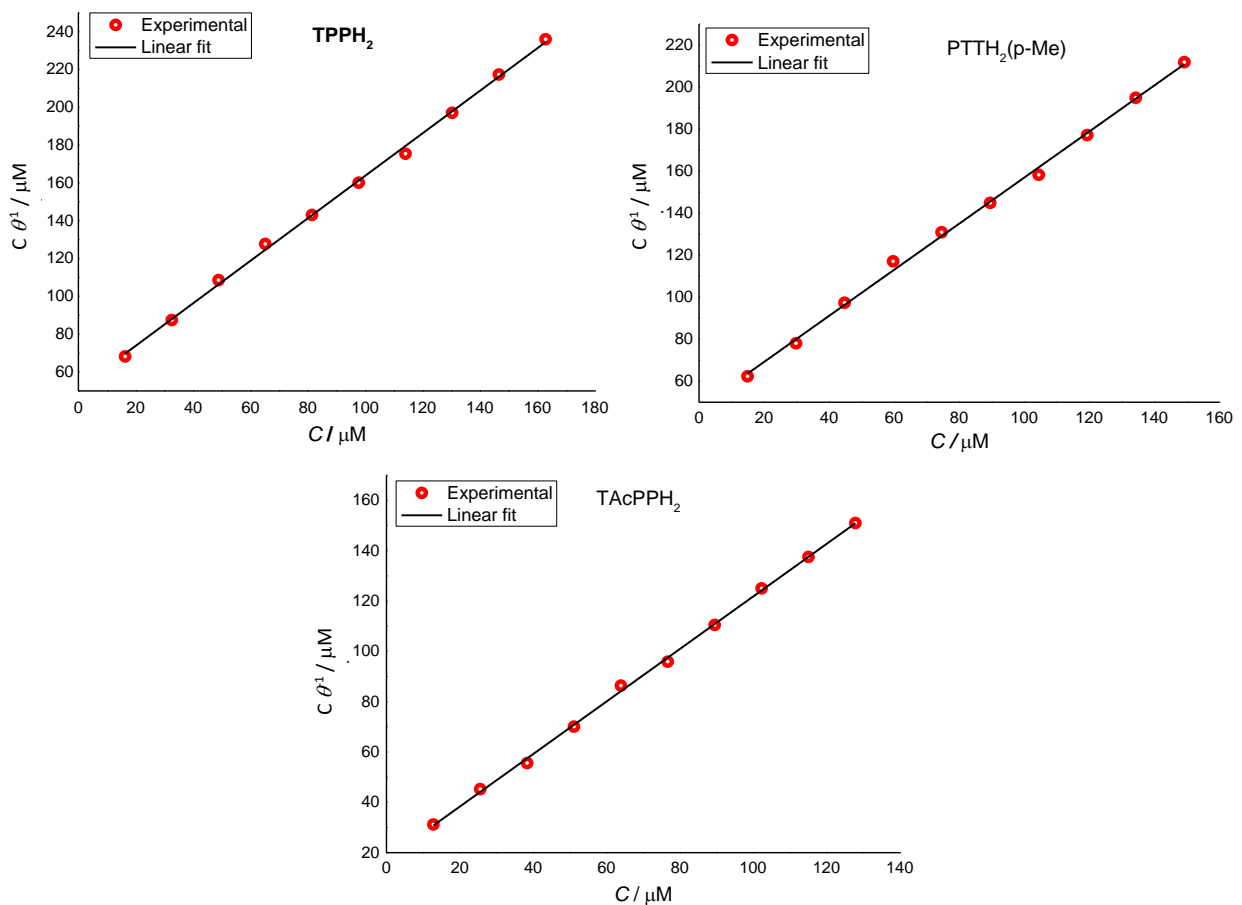


Figure 3. Langmuir’s adsorption plots of TPPH₂, TPPH₂(p-Me) and TAcPPH₂ on mild steel in 0.5 M H₂SO₄ solution

Table 3. Langmuir adsorption isotherm and thermodynamic parameters for adsorption of TPPH₂, TPPH₂(p-Me) and TAcPPH₂ in 0.5 M H₂SO₄ on XC52 mild steel at 25 °C

Molecule	Equation	R ²	K _{ads} / M ⁻¹	ΔG° _{ads} / kJ mol ⁻¹
TPPH ₂	y = 1.1239x + 51.40	0.999	1.94×10 ⁴	-34.4
TPPH ₂ (p-Me)	y = 1.0967x + 46.27	0.999	2.16×10 ⁴	-34.7
TAcPPH ₂	y = 1.0438x + 17.44	0.999	5.73×10 ⁴	-37.1

The standard free energy of adsorption (ΔG°_{ads}) is obtained using the equation (4) [27]:

$$\Delta G^{\circ}_{\text{ads}} = -RT \ln (55.5K_{\text{ads}}) \quad (4)$$

where *R* is the gas constant (8.32 J mol⁻¹K⁻¹) and *T* is absolute temperature (298 K).

The values of ΔG°_{ads} calculated using Eq. (4) are listed in Table 3.

Generally, for ΔG°_{ads} values of around -20 kJ mol⁻¹ or less negative, adsorption is regarded as the physisorption, those around -40 kJ mol⁻¹ or higher, the adsorption is regarded as the chemisorption [28]. In the present study the values of ΔG°_{ads} suggest that adsorption of all studied inhibitors at XC52 mild steel surface is physisorption.

Inhibition mechanism

The mechanism of the corrosion inhibition is generally based on the physical adsorption of inhibitor molecules onto the metal surface. This type of adsorption arises from the electrostatic attractive forces between protonated form of inhibitor molecule and the electrically negative charged surface of the metal. The surface charge of the metal can be attributed to the electric field existing at the metal/solution interface. This surface charge at the open circuit potential can be calculated using the equation (5) [29]:

$$E_r = E_{\text{corr}} - E_{q=0} \quad (5)$$

where *E_r* is referred to as Antropov's rational potential or potential on the correlative scale, *E_{q=0}* is the potential of zero charge, and *E_{corr}* is the corrosion potential. If *E_r* is negative, the electrode surface in this case has a negative net charge and the adsorption of the protonated molecule is favored [26]. The recommended value of PZC in sulphuric acid for mild steel is equal to -0.129 V vs. SCE [30,31]. Nominating this value into eq. (5) and considering *E_{corr}* = -512 mV (Table 2), *E_r* was calculated as -383 mV. The obtained negative value of *E_r* indicates that investigated compounds in 0.5 M sulphuric acid are protonated and subsequently act as cations and adsorb electrostatically on the negatively charged surface of the XC52 mild steel. Note that for any other *E_{corr}* value taken from Table 2, a negative value of *E_r* would also be obtained.

To make evidence of the protonation of porphyrins in the acidic corrosive medium, some UV-vis spectra of TPPH₂, TPPH₂(p-Me) and TAcPPH₂ in DMSO and 0.5 M H₂SO₄ were taken. The obtained electronic absorption spectra (Figure 4) consist of two distinct regions. The first appears at around 410-416 nm which involves the transition from the ground state to the second excited state, and this band is called the Soret band. The second region consists of a weak transition to the first excited state in the range between 512 and 650 nm, and these bands are called the Q bands.

The Soret band of TPPH₂, TPPH₂(p-Me) and TAcPPH₂ in DMSO is centered at 410, 412, and 416 nm respectively, and the Q-bands are all located between 512 and 650 nm [32]. The change in spectra upon addition of diluted acid is attributed to the attachment of protons to two imino nitrogen atoms of the free-base [33].

Other evidence of the physical adsorption of inhibitor onto the XC52 mild steel surface is the increasing of the polarization resistance (*R_p*) upon increasing the inhibitor concentration. The polarization resistance can be calculated using the Stern–Geary equation (6) [34]:

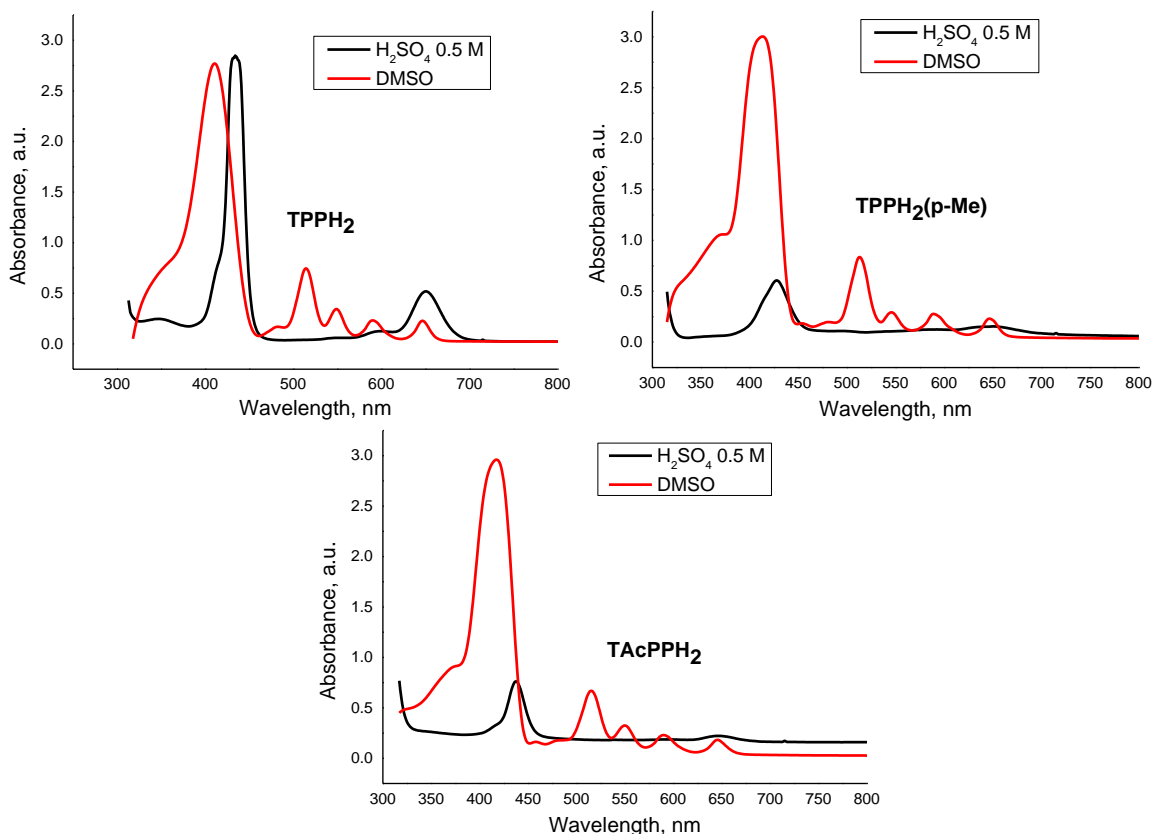


Figure 4. UV-visible spectra of TPPH₂, TPPH₂(p-Me) and TAcPPH₂ in DMSO and 0.5 M H₂SO₄

$$R_p = \frac{\Delta E}{\Delta i} = \frac{\beta_a \beta_c}{2.3(\beta_a + \beta_c) i_{corr}} \tag{6}$$

Table 4 summarized the polarization resistance values obtained from Tafel extrapolation method for selected inhibitor concentrations. The increasing values of the polarization resistance upon increasing the inhibitor concentration reflects adsorption of the inhibitor onto the metal surface which passivates efficiently active sites and inhibits corrosion [35,36].

Table 4. Polarization resistance and Tafel slopes of TPPH₂, TPPH₂(p-Me) and TAcPPH₂ in 0.5 M H₂SO₄

Compound	<i>E</i> _{corr} / mV	β_a / mV dec ⁻¹	β_c / mV dec ⁻¹	<i>R</i> _p / Ω cm ²
30 ppm				
TPPH ₂	-511.3	56	-139.7	47.64
TPPH ₂ (p-Me)	-493.3	62.9	-186.9	62.7
TAcPPH ₂	-484.6	55.9	-159.9	87.66
40 ppm				
TPPH ₂	-512.4	56.8	-139.9	50.79
TPPH ₂ (p-Me)	-495.6	61.4	-191.8	66.08
TAcPPH ₂	-481.3	61.5	-194.3	117.28
50 ppm				
TPPH ₂	-510.0	56.5	-138.4	54.25
TPPH ₂ (p-Me)	-493.4	59.2	-185.4	73.43
TAcPPH ₂	-479.6	62.1	-185.3	128.44
60 ppm				
TPPH ₂	-505.5	53	-147.3	83.5
TPPH ₂ (p-Me)	-489.7	58.1	-176	90.0
TAcPPH ₂	-497.9	56.9	-165.1	162.5

Spectroscopic analysis

UV–visible spectroscopy technique was used to determine the surface adsorption of the inhibitor molecules. The analysis was done before and after each corrosion assay. The UV–vis. spectra of inhibitors in both cases are shown in Figure 5. The inhibitor solutions before the immersion of the metal show adsorption peaks at 452, 439, and 426 nm which correspond to the inhibitors TPPH₂, TPPH₂(p-Me) and TAcPPH₂, respectively. It is clear from Figure 5 that this peak reallocated after the corrosion assessment. All spectra show a remarkable change in the adsorption band, which is associated with adsorption of inhibiting molecules on XC52 mild steel surface [37,38].

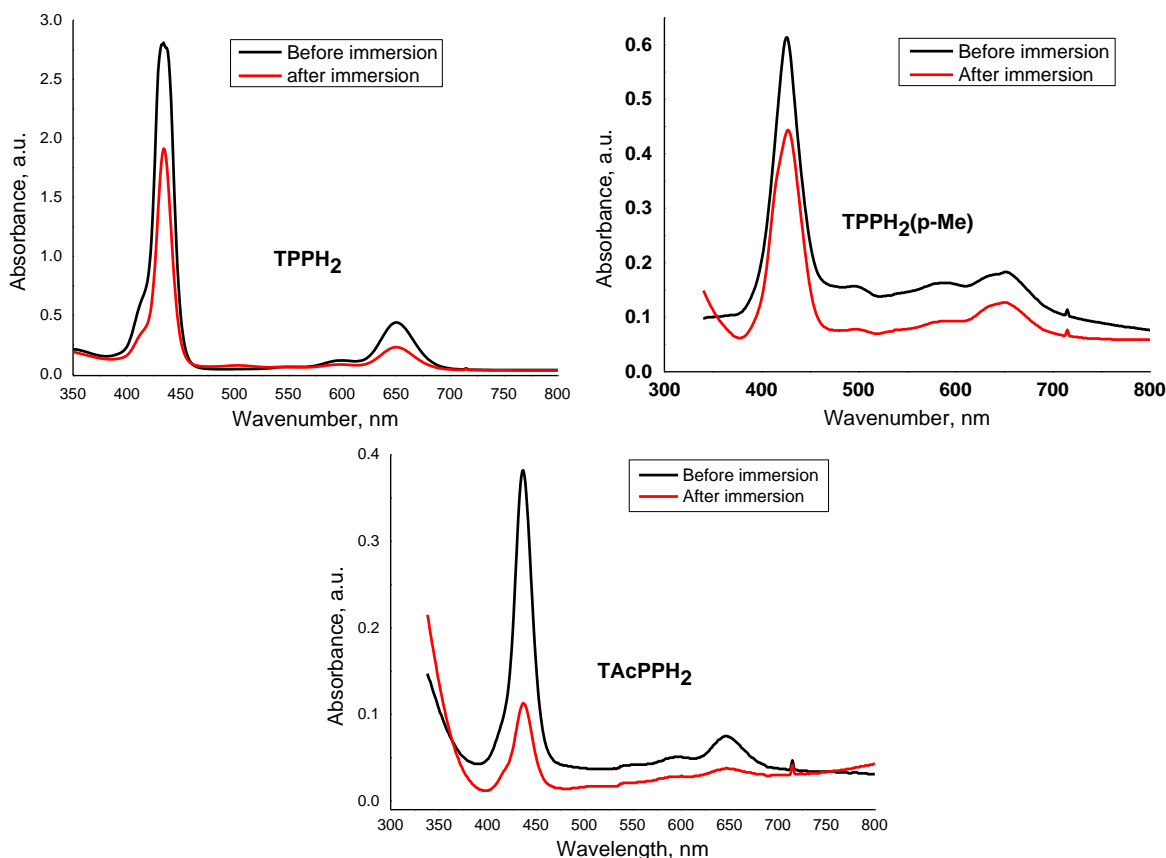


Figure 5. UV–vis spectra of TPPH₂, TPPH₂(p-Me) and TAcPPH₂ before and after immersion of XC52 mild steel specimen in 0.5 M H₂SO₄ for 36 h, at 298 K.

Molecular orbital analysis

The highest occupied molecular orbital energy (E_{HOMO}) and the lowest unoccupied molecular orbital energy (E_{LUMO}) are respectively connected with the electron donating and withdrawing capacities of a compound. The less negative E_{HOMO} and more negative E_{LUMO} are related to low chemical stability and high chemical reactivity because of ease transition of electrons [39]. A smaller energy gap ΔE ($E_{\text{LUMO}} - E_{\text{HOMO}}$) is often interpreted by stronger chemisorption bond and consequently higher inhibition efficiency [40,41].

In order to obtain more information about the frontier molecular orbitals and consequent inhibitory action of the investigated compounds, theoretical study based on molecular orbital analysis was performed. The E_{HOMO} and E_{LUMO} of the investigated compounds were obtained using density functional theory (DFT) without imposing any symmetry constraints, and calculations were realized with the Gaussian 09 package [10]. The exchange functional of Becke and the correlation functional of Lee, Yang and Parr (B3LYP) were employed with 6-311++G(d,p) basis sets. The obtained

contour diagrams of HOMO and LUMO are shown in Figure 6, and the values of the energy of frontier orbitals are reported in Table 5.

According to Figure 6 and data Table 5, the compound TAcPPH₂ has the lowest energy gap value (2.6009 eV) which is the reason for its highest inhibition efficiency. On the other hand, compound TPPH₂(p-Me) has slightly lower energy gap value (2.7056 eV) than TPPH₂ (2.7247 eV), which explains the slightly higher inhibition efficiency of TPPH₂(p-Me) compared to TPPH₂.

Gauss-Sum 2.2 program [42] was used to calculate group contributions to the molecular orbitals (HOMO and LUMO) and prepare the density of states (DOS) plot for the highest and lowest energy gap of TPPH₂, TPPH₂(p-Me) and TAcPPH₂ shown in Figure 7. The DOS spectra were generated by convoluting the molecular orbital information with Gaussian curves of unit height.

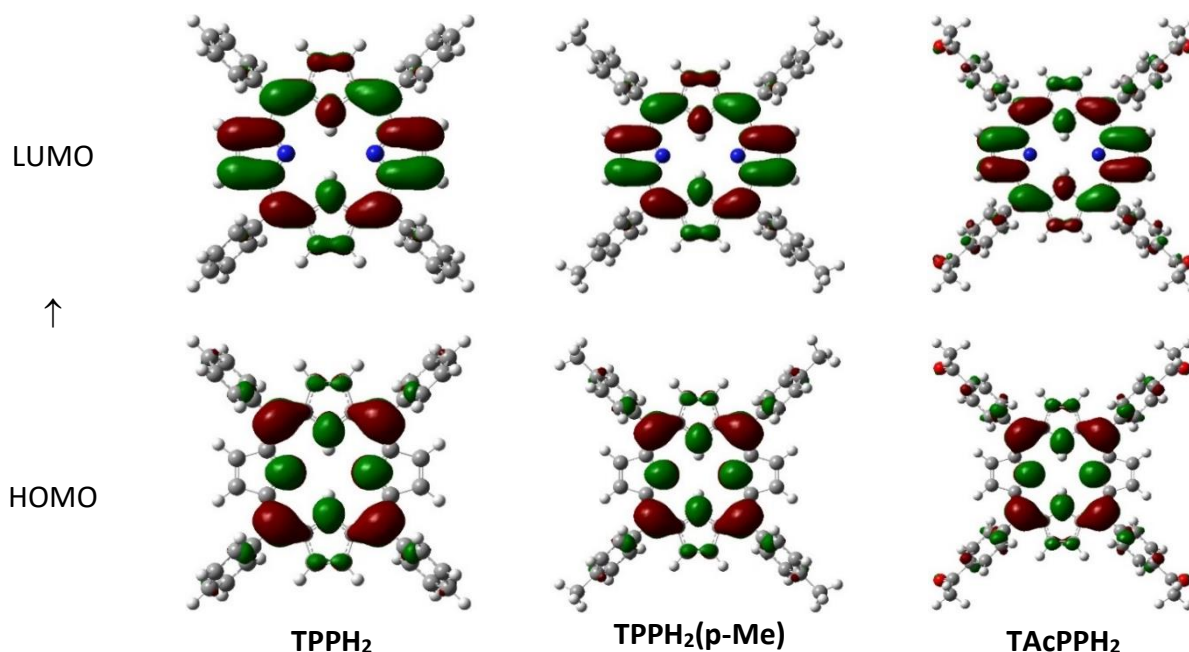


Figure 6. Contour diagrams of HOMO and LUMO of TPPH₂, TPPH₂(p-Me) and TAcPPH₂

Table 5. Energy (eV) of HOMO, LUMO, and energy gap of TPPH₂, TPPH₂(p-Me) and TAcPPH₂.

Parameters	Compounds		
	TPPH ₂	TPPH ₂ (p-Me)	TAcPPH ₂
$E_{\text{HOMO}} / \text{eV}$	-5.2934	-5.1696	-5.5688
$E_{\text{LUMO}} / \text{eV}$	-2.5688	-2.4640	-2.9679
$\Delta E / \text{eV}$	2.7247	2.7056	2.6009

Molecular electrostatic potential map analysis

Molecular electrostatic potential (MEP) map gives an idea about the chemical reactivity of the studied inhibitors. Also, MEP shows the preferred site for the electrophile attack which is colored in red around the amine functions in compounds TPPH₂ and TPPH₂(p-Me). The nitrogen atom in these two compounds is the most preferred site for the nucleophilic attack (Figure 8). The MEP map analysis also shows four red surfaces on each acetyl group of the compound TAcPPH₂, and this may be the reason of high corrosion efficiency of this compound. Figure 8 also shows that the compound TAcPPH₂ shows the maximal negative potential value (-0.0674 a.u.) and the highest positive potentiality value (+0.0674 a.u.).

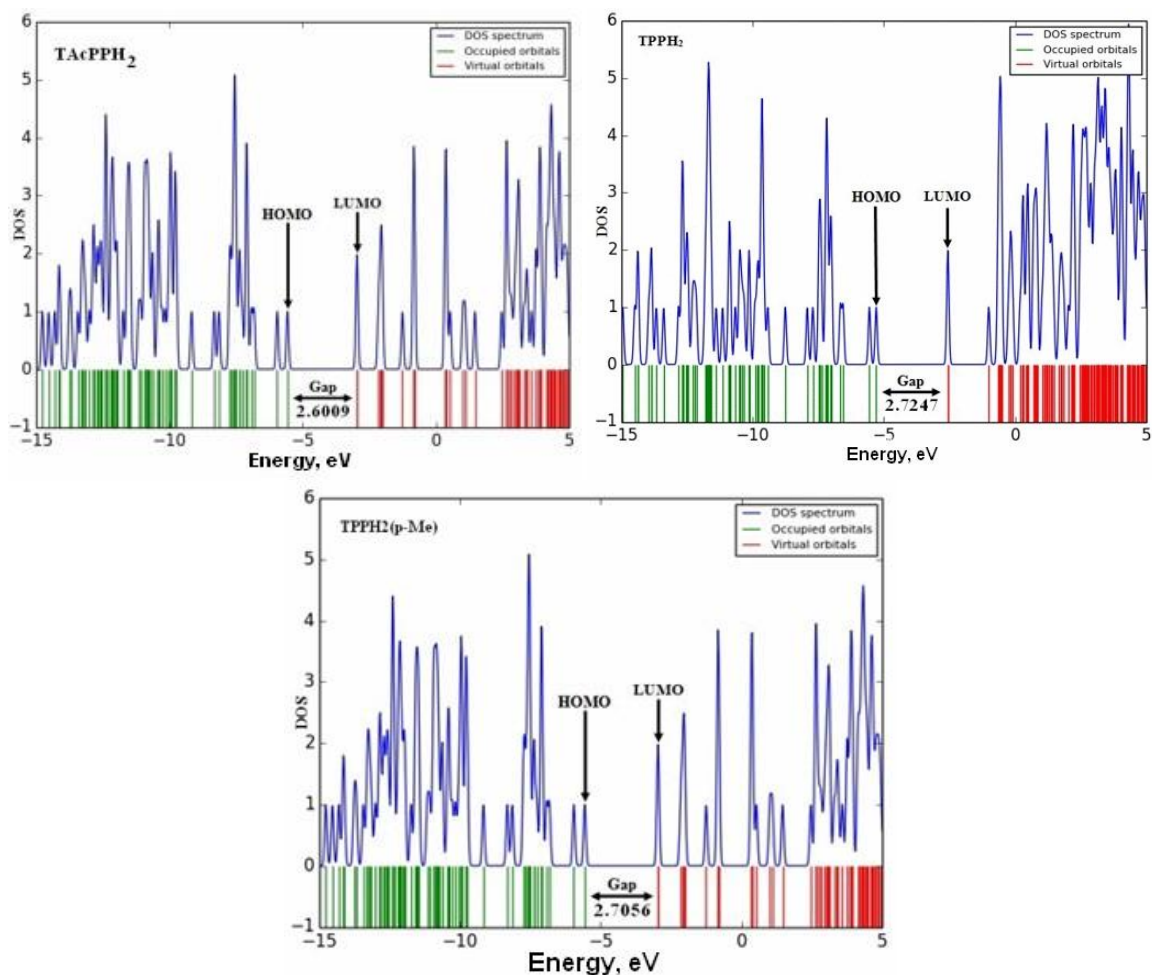


Figure 7. Density of states diagrams and HOMO-LUMO energy gap of TPPH₂, TPPH₂(p-Me) and TAcPPH₂

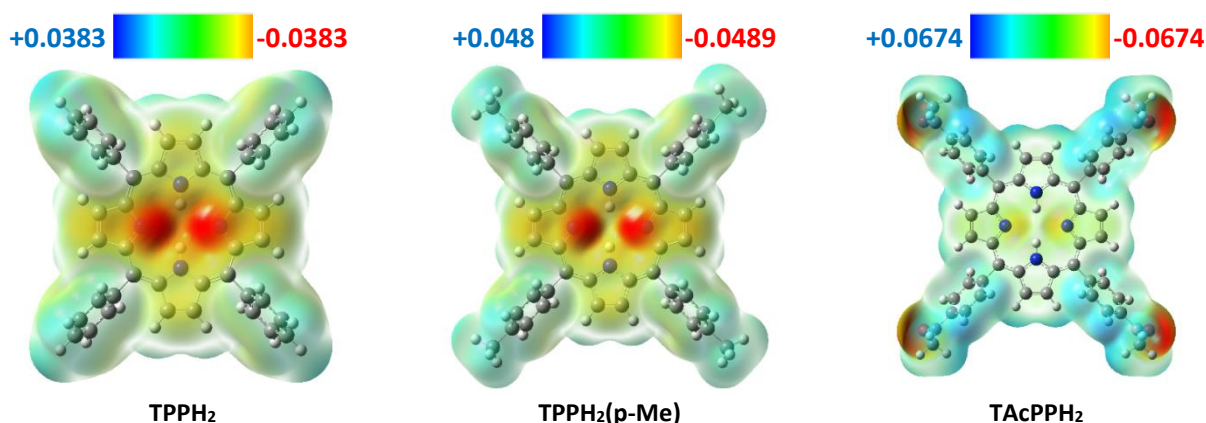


Figure 8. Molecular electrostatic potential map of the studied TPPH₂, TPPH₂(p-Me) and TAcPPH₂ inhibitors

Conclusion

In this work, three meso-tetraphenyl-porphyrin derivatives (TPPH₂, TPPH₂(p-Me) and TAcPPH₂) were tested as corrosion inhibitors of XC52 mild steel in 0.5 M sulphuric acid solution. The results of potentiodynamic polarization showed that the use of TAcPPH₂ can decrease the corrosion of XC52 mild steel by up to 81%, whereas for the TPPH₂ and TPPH₂(p-Me), the inhibition efficiency reaches 65%. Three investigated meso-tetraphenyl-porphyrin derivatives showed dominant anodic reaction. The adsorption of meso-tetraphenyl-porphyrins investigated obeys Langmuir adsorption isotherm. Also, the order of magnitude of adsorption energy indicates that physical adsorption occurs.

The PZC measurement suggested that the mild steel surface was negatively charged in H₂SO₄ solution, and electrostatic interaction was established between adsorbed protonated molecules and negatively charged mild steel surface. Quantum chemical approach was used to calculate HOMO, LUMO, and energy gap using DFT/B3LYP method. The results confirmed a strong bond between meso-tetraphenyl-porphyrins and mild steel surface and suggest a good correlation between calculated quantum chemical parameters and the experimental inhibition efficiency of the inhibitors.

Acknowledgments: The authors gratefully acknowledge the support from the Directorate-General of Scientific Research and Technological Development (DGRSDT) of the Algerian Ministry of Higher Education and Research. Extends thanks to VTRS staff for providing facilities.

References

- [1] F. Javidan, A. Heidarpour, X.L. Zhao, J. Minkinen, *Thin-Walled Structures* **102** (2016) 273-285. <https://doi.org/10.1016/J.TWS.2016.02.002>
- [2] G. Ghosh, P. Rostron, R. Garg, A. Panday, *Engineering Fracture Mechanics* **199** (2018) 609-618. <https://doi.org/10.1016/J.ENGFRACTMECH.2018.06.018>
- [3] D. Dwivedi, K. Lepková, T. Becker, *RSC Advances* **7(8)** (2017) 4580-4610. <https://doi.org/10.1039/C6RA25094G>
- [4] M. Finšgar, J. Jackson, *Corrosion Science* **86** (2014) 17-41. <https://doi.org/10.1016/J.CORSCI.2014.04.044>
- [5] W. Boukhedena, S. Deghboudj, *Journal of Electrochemical Science and Engineering* **11(4)** (2021) 227-239. <http://dx.doi.org/10.5599/jese.1050>
- [6] F. E. Abeng, V. C. Anadebe, P. Y. Nkom, K. J. Uwakwe, E. G. Kamalu, *Journal of Electrochemical Science and Engineering* **11(1)** (2021) 11-26. <http://dx.doi.org/10.5599/jese.887>
- [7] I. A. Kartsonakis, C. A. Charitidis, *Applied Sciences* **10** (2020) 6594. <https://doi.org/10.3390/APP10186594>
- [8] V. G. Sribharathy, S. Rajendran, *Journal of Electrochemical Science and Engineering* **2** (2012) 121-131. <https://doi.org/10.5599/jese.2012.0014>
- [9] C. Zuriaga-Monroy, R. Oviedo-Roa, L.E. Montiel-Sánchez, A. Vega-Paz, J. Marín-Cruz, J.M. Martínez-Magadán, *Industrial and Engineering Chemistry Research* **55** (2016) 3506-3516. https://doi.org/10.1021/ACS.IECR.5B03884/SUPPL_FILE/IE5B03884_SI_001.PDF
- [10] A. Boutarfaia, L. Bechki, T. Lanez, E. Lanez, M. Kadri, *Current Bioactive Compounds* **16** (2019) 1063-1071. <https://doi.org/10.2174/1573407215666191017105239>
- [11] T. Zaiz, T. Lanez, *Journal of Fundamental and Applied Sciences* **4** (2015) 182-191. <https://doi.org/10.4314/JFAS.V4I2.8>
- [12] T. Zaiz, T. Lanez, *Journal of Chemical and Pharmaceutical Research* **4** (2012) 2678-2680.
- [13] M. Frisch, G. Trucks, H. Schlegel, G.S.- Wallingford, U. CT, U. 2009, Gaussian 09; Gaussian Inc, Gaussian, (2016).
- [14] A. D. Becke, *Physical Review A* **38** (1988) 3098-3100. <https://doi.org/10.1103/PhysRevA.38.3098>
- [15] A. D. Becke, *The Journal of Chemical Physics* **98** (1993) 5648-5652. <https://doi.org/10.1063/1.464913>
- [16] B. Miehlich, A. Savin, H. Stoll, H. Preuss, *Chemical Physics Letters* **157** (1989) 200-206. [https://doi.org/https://doi.org/10.1016/0009-2614\(89\)87234-3](https://doi.org/https://doi.org/10.1016/0009-2614(89)87234-3)
- [17] P. M. W. Gill, B. G. Johnson, J. A. Pople, M. J. Frisch, *Chemical Physics Letters* **197** (1992) 499-505. [https://doi.org/10.1016/0009-2614\(92\)85807-M](https://doi.org/10.1016/0009-2614(92)85807-M)
- [18] T. Clark, J. Chandrasekhar, G. W. Spitznagel, P. V. R. Schleyer, *Journal of Computational Chemistry* **4** (1983) 294-301. <https://doi.org/10.1002/JCC.540040303>

- [19] R. Ditchfield, W. J. Hehre, J. A. Pople, *The Journal of Chemical Physics* **54** (1971) 724-728. <https://doi.org/10.1063/1.1674902>
- [20] W. J. Hehre, J. S. Binkley, J. A. Pople, W. J. Pietro, M.S. Gordon, *Journal of the American Chemical Society* **104** (1982) 2797-2803. <https://doi.org/10.1021/JA00374A017>
- [21] M. Birdeanu, C. Epuran, I. Fratilesco, E. Fagadar-Cosma, *Processes* **9** (2021) 1890. <https://doi.org/10.3390/pr9111890>
- [22] M. Behpour, S. M. Ghoreishi, N. Soltani, M. Salavati-Niasari, *Corrosion Science* **51** (2009) 1073-1082. <https://doi.org/10.1016/J.CORSCI.2009.02.011>
- [23] M. W. Khalil, *Materials Science & Engineering Technology* **23** (1992) 111-115. <https://doi.org/10.1002/mawe.19920230311>
- [24] J. Ge, O. B. Isgor, *Materials and Corrosion* **58** (2007) 573-582. <https://doi.org/10.1002/maco.200604043>
- [25] M. Christov, A. Popova, *Corrosion Science* **46** (2004) 1613-1620. <https://doi.org/10.1016/J.CORSCI.2003.10.013>
- [26] P. Li, J.Y. Lin, K.L. Tan, J.Y. Lee, *Electrochimica Acta* **42** (1997) 605-615. [https://doi.org/10.1016/S0013-4686\(96\)00205-8](https://doi.org/10.1016/S0013-4686(96)00205-8)
- [27] A. Popova, M. Christov, *Journal of the University of Chemical Technology and Metallurgy* **43(1)** (2008) 37-47.
- [28] T. Benabbouha, M. Siniti, H. El Attari, K. Chefira, F. Chibi, R. Nmila, H. Rchid, *Journal of Bio- and Tribo-Corrosion* **4** (2018) 39. <https://doi.org/10.1007/s40735-018-0161-0>
- [29] L. I. Antropov, *Zhurnal Fizicheskoi Khimii* **37** (1963) 965-978.
- [30] I. A. Ammar, F. M. El Khorafi, *Materials and Corrosion* **24** (1973) 702-707. <https://doi.org/10.1002/MACO.19730240806>
- [31] E. E. Mola, *Electrochimica Acta* **26** (1981) 1209-1217. [https://doi.org/10.1016/0013-4686\(81\)85101-8](https://doi.org/10.1016/0013-4686(81)85101-8)
- [32] D. Swain, A. Rana, P.K. Panda, S.V. Rao, *Chemical Physics Letters* **610** (2014) 310-315. <https://doi.org/10.1016/j.cplett.2014.07.013>
- [33] R. Giovannetti, L. Alibabaei, F. Pucciarelli, *Inorganica Chimica Acta* **363(7)** (2010) 1561-1567. <https://doi.org/10.1016/j.ica.2009.12.015>
- [34] L. Larabi, Y. Harek, M. Traisnel, A. Mansri, *Journal of Applied Electrochemistry* **34** (2004) 833-839. <https://doi.org/10.1023/B:JACH.0000035609.09564.E6>
- [35] F. Mansfeld, *Corrosion* **37** (1981) 301-307. <https://doi.org/10.5006/1.3621688>
- [36] F. Mohsenifar, H. Jafari, K. Sayin, *Journal of Bio- and Tribo-Corrosion* **2** (2016) 1. <https://doi.org/10.1007/s40735-015-0031-y>
- [37] I. Fratilesco, A. Lascu, B.O. Taranu C. Epuran, M. Birdeanu, A. Macsim, E. Tanasa, E. Vasile, E. Fagadar-Cosma, *Nanomaterials* **12** (2022) 1930. <https://doi.org/10.3390/nano12111930>
- [38] A. Dehghani, G. Bahlakeh, B. Ramezanzadeh, M. Ramezanzadeh, *Journal of the Taiwan Institute of Chemical Engineers* **100** (2019) 239-261.
- [39] M. Uzzaman, M.K. Hasan, S. Mahmud, A. Yousuf, S. Islam, M.N. Uddin, A. Barua, *Informatics in Medicine Unlocked* **25** (2021) 100706. <https://doi.org/10.1016/J.IMU.2021.100706>
- [40] R. G. Parr, Z. Zhou, *Accounts of Chemical Research* **26** (2002) 256-258. <https://doi.org/10.1021/AR00029A005>
- [41] P.W. Ayers, R.G. Parr, R.G. Pearson, *The Journal of Chemical Physics* **124** (2006) 194107. <https://doi.org/10.1063/1.2196882>
- [42] N. M. O'Boyle, A. L. Tenderholt, K. M. Langner, *Journal of Computational Chemistry* **29** (2008) 839-845. <https://doi.org/10.1002/JCC.20823>

©2022 by the authors; licensee IAPC, Zagreb, Croatia. This article is an open-access article distributed under the terms and conditions of the Creative Commons Attribution license (<https://creativecommons.org/licenses/by/4.0/>)